f_{LT} response function of ^{2}H$(e, e'p)n$ at $Q^2 = 0.33$ (GeV/c)^2

W. U. Boeglin,[*] H. Arenhövel, K. I. Blomqvist,[†] R. Böhm, M. Distler, R. Edelhoff, I. Ewald,[‡] R. Florizone,[§] J. Friedrich, R. Geiges, M. Kahrau, M. Korn, H. Kramer,[‖] K. W. Krygier, V. Kunde,[¶] A. Liesenfeld, K. Merle, R. Neuhausen, E. A. J. M. Offermann,[**] Th. Pospischil, A. W. Richter,[‖] G. Rosner,[††] P. Sauer,[‖] S. Schardt, A. Serdarevic,[‡‡] A. Wagner, Th. Walcher, and S. Wolf
Institut für Kernphysik, Johannes Gutenberg-Universität, J.J.-Becher-Weg 45, D-55099 Mainz, Germany

J. Jourdan and I. Sick
Departement für Physik und Astronomie, Universität Basel, CH-4056 Basel, Switzerland

M. Kuss[§§]
Institut für Kernphysik, TH Darmstadt, D-64289 Darmstadt, Germany

M. Potokar, A. Rokavec, B. Vodenik, and S. Sirca
Institute Jožef Stefan, University of Ljubljana, SI-61111 Ljubljana, Slovenia
(Received 27 May 2008; revised manuscript received 9 September 2008; published 5 November 2008)

The interference response function $f_{LT}(R_{LT})$ of the ^{2}H$(e, e'p)n$ reaction has been determined at squared four-momentum transfer $Q^2 = 0.33$ (GeV/c)^2 and for missing momenta up to $p_m = 0.29$ GeV/c. The results have been compared to calculations that reproduce f_{LT} quite well but overestimate the cross sections by 10–20% for missing momenta between 0.1 GeV/c and 0.2 GeV/c.

DOI: 10.1103/PhysRevC.78.054001 PACS number(s): 25.30.Fj, 25.10.+s, 25.60.Gc

I. INTRODUCTION

The deuteron is an ideal system to investigate fundamental problems in nuclear physics such as the ground state and continuum wave functions and the structure of the electromagnetic current operator. In addition, interaction effects such as meson exchange currents (MEC), and isobar configurations (IC) can be studied.

The deuteron structure can be calculated with very high accuracy therefore providing a testing ground for various models of the nucleon-nucleon force and subnuclear degrees of freedom.

The exclusive deuteron electrodisintegration cross section has been measured at several laboratories during the past 25 years (references to these experiments can be found in the text below). However there are only a few experiments where the individual response functions have been separated. In this paper we report a measurement of the $f_{LT}(R_{LT})$ response function, extending the kinematic area where experimental data are available.

The ^{2}H$(e, e'p)n$ reaction can be most easily interpreted within the framework of the plane wave impulse approximation (PWIA). In this approximation the cross section is written as follows:

$$\frac{d^5\sigma}{d\omega d\Omega_e d\Omega_p} = \kappa \cdot \sigma_{ep} \cdot S(p_i). \quad (1)$$

Here, σ_{ep} describes the elementary electron proton (off-shell) cross section for scattering an electron off a moving bound proton [1]. The factor κ is a kinematic factor, and $S(p_i)$ is the spectral function which describes the probability of finding a proton with an initial momentum p_i. In this approximation, the initial momentum of the proton is opposite and equal in magnitude to the missing momentum p_m, the momentum of the recoiling, non-observed neutron.

Several experiments explored the ^{2}H$(e, e'p)n$ cross section over a wide range of missing momenta at small to medium momentum transfers [2–5]. The focus of these measurements was the exploration of the momentum distribution within the plane wave impulse approximation (for a theoretical analysis of the Saclay experiment [2] see [6]). It has been found, however, that with increasing missing momentum final state interactions (FSI) and, related to the corresponding energy transfer, MEC and IC contributions increase dramatically. Figure 1 shows the ^{2}H$(e, e'p)n$ cross section measured at MAMI [4] together with a calculation that includes FSI, MEC, and IC [7]. One can see that the cross section is well reproduced up to $p_m = 350$ MeV/c by a calculation that includes FSI.

[*]Present Address: Florida International University, Miami, Florida USA.
[†]Present address: DANFYSIK, Jyllinge, Denmark.
[‡]Present address: Renewable Energies, Koenig-Konrad-Strasse 2, D-55127 Mainz, Germany.
[§]Present address: Canadian Light Source Inc., University of Saskatchewan, 101 Perimeter Road, Saskatoon, SK, Canada S7N 0X4.
[‖]Present address: TLC GmbH, Wiesbaden, Germany.
[¶]Present address: Mannesmann Autocom, Düsseldorf, Germany.
[**]Present address: Renaissance Technologies, Stony Brook, New York, USA.
[††]Present address: Department of Physics and Astonomy, University of Glasgow, Glasgow, G128QQ, Scotland, UK.
[‡‡]Present address: 126 Cliff Rd, Port Jefferson, NY, USA.
[§§]Present address: INFN Pisa, Italy.

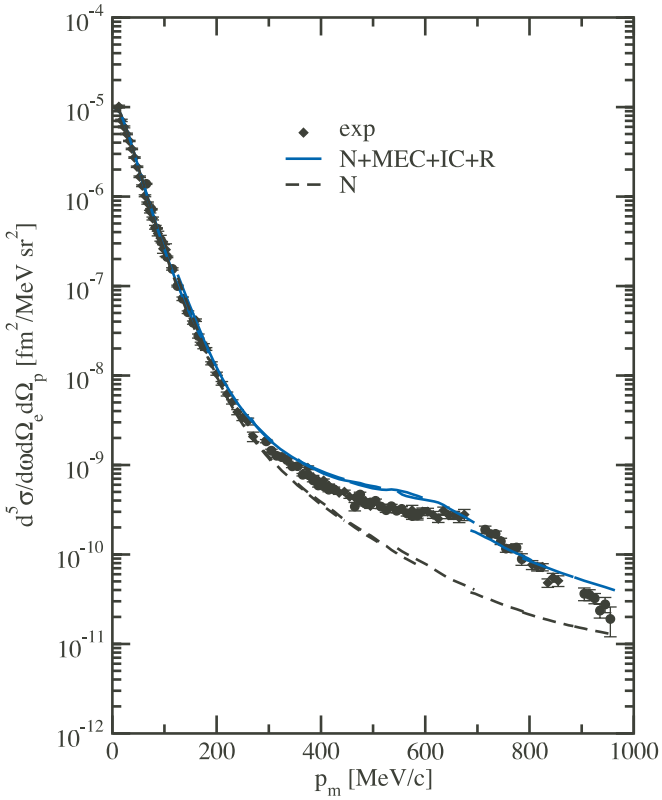

FIG. 1. (Color online) The experimental ^{2}H$(e, e'p)n$ cross section as a function of missing momentum measured at MAMI for $Q^2 = 0.33$ (GeV/c)^2 [4] compared to calculations [7] with (solid curve) and without (dashed curve) meson exchange currents (MEC) and isobar currents (IC). Both calculations used the Paris potential and include FSI (N) and leading order relativistic corrections (R). The low p_m data have been re-analyzed and used in this work to determine f_{LT}.

At higher p_m there are significant discrepancies between experiment and the FSI calculation. If additionally MEC and IC are included the agreement improves considerably but significant discrepancies remain. The largest deviations occur at energy transfers where large virtual delta excitation contributions are expected.

When these additional contributions are taken into account the cross section cannot be factorized in this simple way anymore and one has to use the full one photon exchange approximation. Within this limit, the $(e, e'p)$ cross section can be written as follows:

$$\frac{d^5\sigma}{d\omega^{\rm lab} d\Omega_e^{\rm lab} d\Omega_p^{\rm lab}} = \sigma_{\rm Mott}(v_L R_L + v_T R_T + v_{LT} R_{LT} \cos\phi + v_{TT} R_{TT} \cos 2\phi). \quad (2)$$

The functions R_x ($x \in \{L, T, LT, TT\}$) are response functions and the factors v_x ($x \in \{L, T, LT, TT\}$) are kinematic factors depending on the electron kinematics only. For a detailed discussion see Refs. [8–10]. The response functions consist of combinations of transition matrix elements of the components of the electromagnetic current operator and contain the structure information; the incident and the scattered electrons are described as plane waves. The angle ϕ is the angle between the electron scattering plane and the reaction plane, defined by the momentum of the ejected nucleon and the momentum transfer.

For the following discussion, $\theta_{np}^{\rm c.m.}$ represents the angle between the proton momentum vector and the momentum transfer vector in the center of mass of the np-system, and θ_e is the electron scattering angle in the laboratory frame.

In view of the fact that the theoretical calculation [7] is based on an evaluation of the responses in the final np-c.m. system using the following form of the differential cross section (note that $\phi = \phi_{np}^{\rm c.m.}$)

$$\frac{d^5\sigma}{d\omega^{\rm lab} d\Omega_e^{\rm lab} d\Omega_{np}^{\rm c.m.}} = C\left(\rho_L f_L(\theta_{np}^{\rm c.m.}) + \rho_T f_T(\theta_{np}^{\rm c.m.}) + \rho_{LT} f_{LT}(\theta_{np}^{\rm c.m.}) \cos\phi_{np}^{\rm c.m.} + \rho_{TT} f_{TT}(\theta_{np}^{\rm c.m.}) \cos 2\phi_{np}^{\rm c.m.}\right), \quad (3)$$

we now switch to the response functions f_x with $x \in \{L, T, LT, TT\}$. Using the relations

$$C = \frac{\eta}{6\pi^2 \alpha Q^2} \sigma_{\rm Mott}, \quad (4)$$

where α denotes the fine structure constant and $\eta = \tan^2(\theta_e/2)$, and

$$\rho_L = \tilde{\beta}^2 \frac{Q^2}{2\eta} v_L, \quad \rho_T = \frac{Q^2}{2\eta} v_T, \quad \rho_{LT} = \tilde{\beta} \frac{Q^2}{2\eta} v_{LT}, \quad \rho_{TT} = \frac{Q^2}{2\eta} v_{TT}, \quad (5)$$

where $\tilde{\beta} = \frac{q_{\rm lab}}{q_{\rm c.m.}}$ expresses the boost from the laboratory to the c.m. system, one obtains the relations between the response functions R_x and the f_x as follows:

$$\frac{\tilde{\beta}^2 \mathcal{J}}{12\pi^2\alpha} f_L = R_L, \quad \frac{\tilde{\beta}\mathcal{J}}{12\pi^2\alpha} f_{LT} = R_{LT}, \quad \frac{\mathcal{J}}{12\pi^2\alpha} f_T = R_T, \quad \frac{\mathcal{J}}{12\pi^2\alpha} f_{TT} = R_{TT}, \quad (6)$$

with $\mathcal{J} = |\partial\Omega_{np}^{\rm c.m.}/\partial\Omega_p^{\rm lab}|$ as Jacobian.

A full separation of all four response functions requires at least one cross section to be measured with the proton detected out of the electron scattering plane. This has been achieved at MIT-Bates using the Out-Of-Plane spectrometer (OOPS) system [11] and at NIKHEF [12] using the HADRON detectors. For an overview of results see [13].

Simpler in-plane measurements allow one to separate, f_L, f_T, and f_{LT}. The response function which is easiest to determine is f_{LT} since in this case the electron momentum can remain constant, and one only has to scan the proton momentum such that the $(e, e'p)$ cross sections can be measured at $\phi = 0°$ and at $\phi = 180°$.

In-plane separations have been carried out at missing momenta between 0 and 220 MeV/c and at lower Q^2 values at several laboratories and the published results can be found in references [14–17]. The momentum transfer dependence of f_L, f_T, and f_{LT} has been measured at Saclay for missing momenta between 0 and 150 MeV/c [18]. At SLAC, cross sections and f_{LT} have been determined at large momentum transfers for missing momenta up to 200 MeV/c [19].

In this paper we report on the determination of f_{LT} close to the quasifree peak (for Bjorken variable $0.84 < x < 1$), at an average Q^2 of 0.33 (GeV/c)^2 for missing momenta up to 290 MeV/c.

II. EXPERIMENTAL DETAILS

The experiment has been carried out at the three-spectrometer facility [20] at the Mainz microtron MAMI using spectrometer B to detect electrons and spectrometer A to measure protons. The incident beam energy was $E_{\rm inc} =$ 855.11 MeV, and the electron scattering angle was kept constant at $\theta_e = 45^\circ$. The momentum acceptance of the electron spectrometer was $\Delta p/p = \pm 7.4\%$ and the one of the proton spectrometer $\Delta p/p = -5, +15\%$ with respect to the corresponding reference momenta. The rectangular entrance slit of the electron spectrometer defined an angular acceptance of $\Delta\theta_e = \pm 20$ mr in the scattering (horizontal) plane, and $\Delta\phi_e = \pm 70$ mr in the vertical plane. The proton spectrometer had an acceptance of $\Delta\theta_p = \pm 75$ mr (horizontal) and $\Delta\phi_p = \pm 70$ mr (vertical). The momenta of the outgoing protons varied between 531 MeV/c and 627 MeV/c.

For the determination of f_{LT}, three spectrometer settings were selected for each central value of $\phi = 0^\circ$ and $\phi = 180^\circ$ and one setting where the proton spectrometer was centered around the direction of $\vec{q}$.

These proton spectrometer settings corresponded to the center of mass angles $\theta_{np}^{\rm c.m.} = 0^\circ, 20^\circ, 40^\circ$, and 48°. For a given, fixed electron kinematics, a variation of $\theta_{np}^{\rm c.m.}$ also corresponds to a change of the missing momentum. The relation between $\theta_{np}^{\rm c.m.}$ and p_m for this experiment is shown in Fig. 2. The central settings of the spectrometers are listed in Table I.

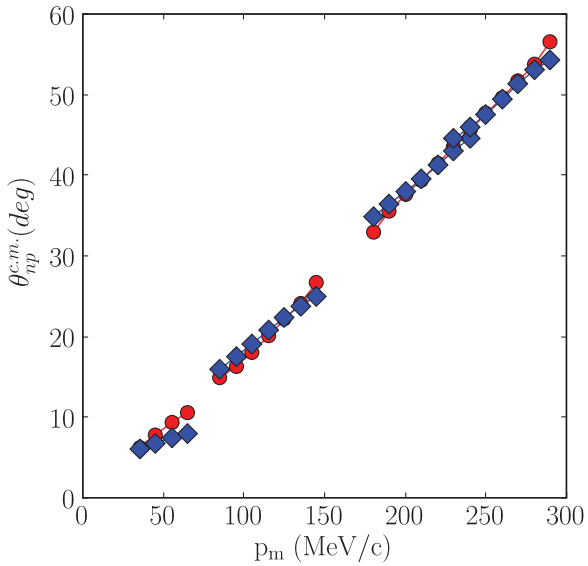

FIG. 2. (Color online) The relation between missing momentum and the angle between the ejected proton and the momentum transfer in the center of mass for kinematics I–VIII. The red circles correspond to the spectrometer settings centered around $\phi = 0^\circ$ and the blue diamonds correspond to $\phi = 180^\circ$. All points within the kinematic acceptance of a single spectrometer setting are joined by a line.

TABLE I. Central spectrometer settings.

Kinematics	θ_e (°)	p_e (MeV/c)	θ_p (°)	p_p (MeV/c)
I	45.00	657.1	49.85	608.4
II	45.00	657.2	39.84	599.1
III	45.00	657.6	29.68	569.5
IV	45.00	656.0	25.17	554.0
V	45.00	657.1	49.85	608.4
VI	45.00	657.2	59.98	599.1
VII	45.00	657.6	70.13	569.5
VIII	45.00	657.5	74.54	551.3

The energy and momentum transfer, ω and $\vec{q}$ were kept constant, centered at 200 MeV and at 600 MeV/c, respectively. Both of these quantities varied slightly by a few MeV/c due to the large acceptances of the spectrometers. The maximum value of $\theta_{np}^{\rm c.m.}$ was determined by the smallest angle with respect to the beam, that the out-going protons could be detected for the given electron kinematics. A detailed list of kinematics can be found in the Appendix in Tables III–X.

We used a liquid-deuterium target consisting of a cylindrical target cell with a diameter of 2 cm made of HAVAR and a wall thickness of 6.5 μm or 10 mg/cm^2. The deuterium target thickness was 310 mg/cm^2. The liquid deuterium was continuously circulated by means of an immersed fan, thus preventing the liquid at the intersection with the electron beam from boiling. Since the beam diameter was typically of the order of 0.2 mm, the beam was rastered horizontally by ± 3.5 mm and vertically by ± 2.5 mm with a frequency of 3.5 kHz horizontally and 2.5 kHz vertically to further reduce the risk of boiling. The current in the raster coil was measured on an event by event basis which allowed us to reconstruct the beam position for each event in order to correct for energy losses in the target. After applying the necessary kinematic corrections we obtained at low missing momenta a missing energy resolution of 0.45 MeV (FWHM) which degraded to 2 MeV with increasing missing momentum, as one has to include increasingly large kinetic energies of the recoiling neutron in the calculation of the missing energy. With this target system, beam currents between 2 μA and 40 μA could be used.

The effective target thickness has been determined using elastic scattering via ^{2}H$(e, e'^2$H) measurements where the scattered electrons and the recoiling deuterons where detected in coincidence. The ^{2}H$(e, e'^2$H) coincidence cross sections were then compared to the single arm (^{2}H$(e, e')^2$H) elastic scattering cross sections of Platchkov *et al.* [21] and Auffret *et al.* [22] to extract the cross section normalization factor as a function of electron beam current. These normalization measurements were performed in regular intervals during the experiment. From fitting a line to the ratio of the measured elastic cross section in this experiment to the Saclay data, we found a current dependence of the target thickness of $0.1\%/\mu$A (Fig. 3).

The normalization factor varied between 1.082 at 5 μA and 1.12 at 40 μA. Contributions to this factor are the change of the effective target thickness due to the horizontal rastering of the beam position (4%), the 3% hydrogen admixture to the

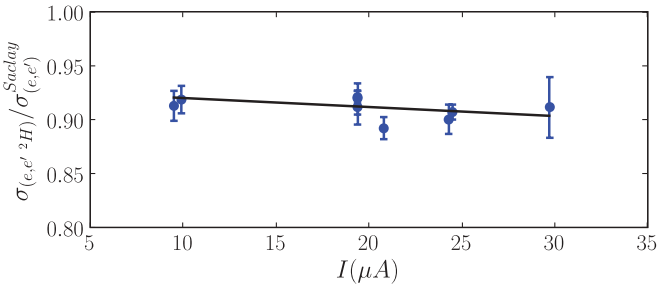

FIG. 3. (Color online) The ratio between the ^{2}H$(e, e'^2$H) elastic (coincidence) cross section from this experiment and the interpolated elastic (single arm) cross sections, measured at ALS in Saclay [21,22]. This ratio has been used to normalize all coincidence cross sections.

deuterium gas, and losses of recoil deuterons due to nuclear reactions in the target material, estimated to be less than 3%.

The systematic error of the measured cross sections has been determined to be about 6.2%. It contains contributions from the uncertainty in the elastic deuteron cross section (2%), estimated deuteron losses (2.5%) and the uncertainty of the normalization factor due to the statistical error in the ^{2}H$(e, e'^2$H) cross section (1.7%).

The error due to the uncertainties in the kinematic variables such as beam energy, beam direction, electron momentum and direction and proton direction was estimated for each bin. Their values lie between 0.3% and 4% depending on the kinematics. The largest errors are found for the setting where the protons are almost parallel (central setting where $\theta_{np}^{\text{c.m.}} = 0^\circ$) to the momentum transfer and the $(e, e'p)$ cross section is dominated by f_L and f_T. For this setting the experimental cross sections were dominated by statistical errors and the extracted f_{LT} provides just an upper limit. For the next setting ($\theta_{np}^{\text{c.m.}} \geqslant 20^\circ$) they are of the order of 1% and below for the rest of the data. We have added these errors in quadrature to the statistical ones.

III. DETERMINATION OF f_{LT}

In order to extract the cross sections, the data have been binned in two dimensions, missing energy and missing momentum. The spectra have subsequently been radiatively unfolded and corrected for the coincidence phase space acceptance. For each bin in missing momentum, we obtained the cross section by integrating over missing energy, where the ^{2}H$(e, e'p)n$ reaction produces a peak at 2.25 MeV.

The large acceptances of the spectrometers lead to large regions in the kinematic variables that have been sampled at each spectrometer setting. Cuts in $\vec{q}, \omega, \theta_{pq}$ (the angle between the ejected proton and the momentum transfer in the laboratory frame), and ϕ have been applied (Fig. 4 and Table II) in order to have well defined kinematic regions sampled in each spectrometer setting. In addition to these global kinematic cuts, the smaller kinematic regions contributing to each missing momentum bin within a spectrometer setting need to be analyzed. For this analysis we used the same Monte Carlo program as has been employed to determine the phase space acceptance (necessary to determine the coincidence cross section) and included the full theoretical cross section to

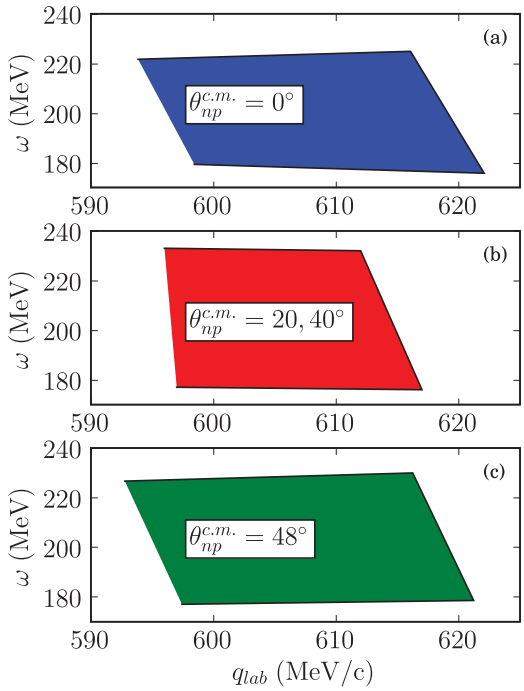

FIG. 4. (Color online) Cuts in q_{lab} and ω applied to the different kinematic settings [(a) I, (b) II, III, (c) IV see Table I]. The same cuts have been applied to the corresponding $\phi = 180^\circ$ settings.

estimate the yield. The distributions of the various kinematic variables obtained from the Monte Carlo simulation agree well with the experimental ones. As an example Fig. 5 shows the relevant kinematic variables of the coincidence cross section for kinematic setting VIII. The points with error bars are the experimental values and the solid (red) line is the calculated distribution, scaled to reproduce the experimental yield. In addition experimental distributions of q_{lab} and ω for $\phi \approx 0^\circ$ and $\phi \approx 180^\circ$ are shown in Fig. 6. These distributions contain all missing momenta accessible by each spectrometer setting. While the distributions for the momentum transfer are quite similar, considerably larger variations can be observed for ω. As a consequence one finds larger variations in the average ω for each missing momentum bin between the two ϕ settings (Fig. 7).

We determined the average of the following kinematic variables for each missing momentum bin: the electron scattering angle (θ_e), the momentum and energy transfers ($\omega_{\text{lab}}, q_{\text{lab}}$) and

TABLE II. Angle cuts applied at the kinematic settings

Kinematics	ϕ_{min} (°)	ϕ_{max} (°)	$\theta_{pq_{\text{min}}}$ (°)	$\theta_{pq_{\text{max}}}$ (°)
I	−60	60	1	10
II	−35	35	5	15
III	−15	15	15	25
IV	−15	15	20	30
V	120	240	1	10
VI	145	215	5	15
VII	165	195	15	25
VIII	165	195	20	30

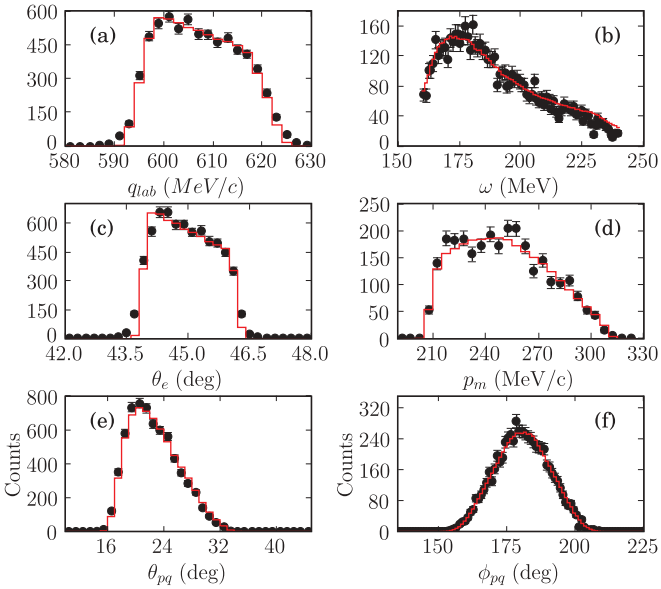

FIG. 5. (Color online) Comparison of the distribution of kinematic variables between the experiment and the Monte Carlo calculation for kinematic setting VIII: (a) momentum transfer, (b) energy transfer, (c) electron scattering angle, (d) missing momentum, (e) angle between the proton momentum and the momentum transfer, and (f) the angle between the reaction plane and the electron scattering plane. Note: $\phi_{pq} = \phi_{np}^{\text{c.m.}} = \phi$.

the final proton momentum p_f. From these averaged quantities and the missing momentum we subsequently calculated the average angle between the outgoing proton and the momentum transfer θ_{pq}. This quantity could also have been obtained directly from the Monte Carlo calculation; however, the ^{2}H$(e, e'p)n$ kinematics would then have been over-determined

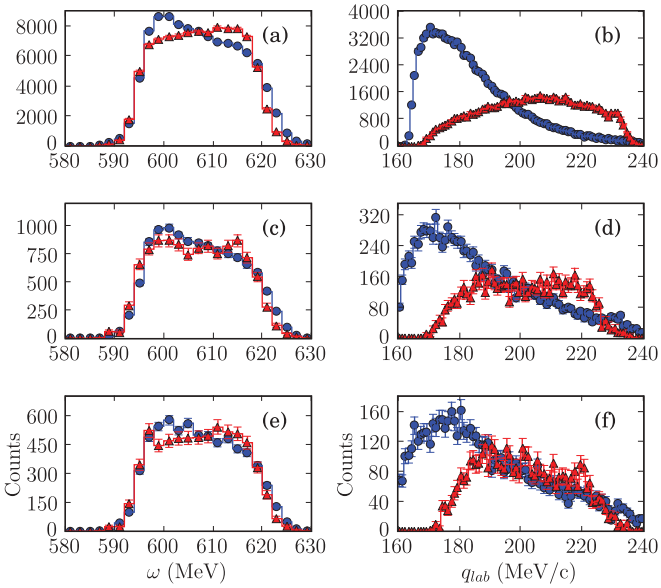

FIG. 6. (Color online) Comparison of the distribution of q_{lab} and ω for kinematic setting II and VI (a,b) for setting III and VII (c,d) and for setting kinematic IV and VIII (e,f). The (red) circles correspond to $\phi \approx 0^\circ$ and the (blue) triangles correspond to $\phi \approx 180^\circ$.

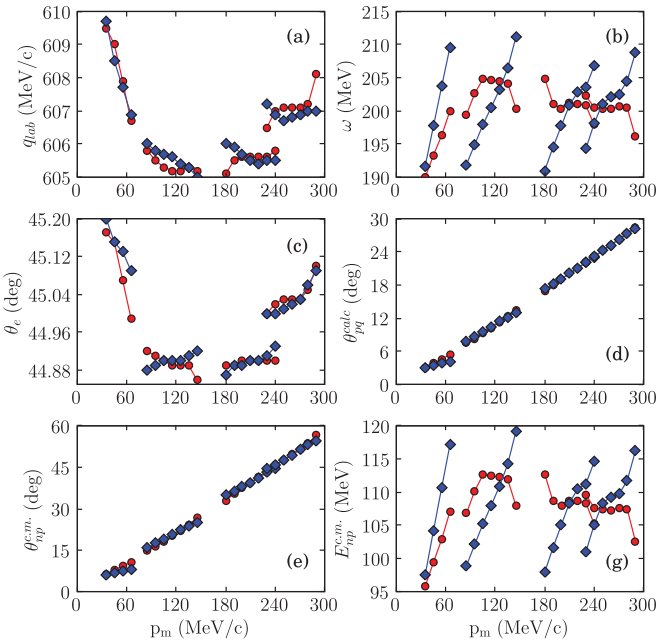

FIG. 7. (Color online) Averaged kinematic variables as a function of missing momentum: three-momentum transfer in the lab frame (a), energy transfer (b), electron scattering angle (c), proton angle with respect to the momentum transfer in the lab (d) and in the center of mass frame (e), total energy in the center of mass (f). The red circles correspond to $\phi = 0^\circ$ and the blue diamonds correspond to $\phi = 180^\circ$. Points that are joined by a line are part of the same spectrometer setting.

and the averaging process would have resulted in inconsistent kinematic values. We therefore selected to calculate the average value of θ_{pq} from the averaged values for p_f, q_{lab} and p_m. The average kinematic variables as a function of missing momentum are shown in Fig. 7.

From the same calculation we also obtained the averaged values for the Mott cross section, the recoil factor (due to the four-momentum conserving delta function [8,9]), the kinematic factors for the response functions [i.e., the density matrix for the virtual photon polarization ρ_x, in Eq. (3)] and averages of $\cos\phi$ and $\cos 2\phi$. ρ_x can also be calculated from the averaged kinematic values associated with each data bin.

From the general ^{2}H$(e, e'p)n$ cross section in Eq. (3) one sees that the interference response functions can be extracted from the ϕ dependence of the cross section. Most of the data taken in this experiment are in or close to the electron scattering plane, with ϕ angles distributed around $\phi = 0^\circ$ and $\phi = 180^\circ$. We have decided to extract f_{LT} from the cross section difference:

$$\sigma_{LT} = \frac{1}{\overline{\cos\phi_0} - \overline{\cos\phi_1}}(\sigma_0 - \sigma_{180}), \tag{7}$$

$$\sigma_{LT} = C_{\text{tot}} \cdot \overline{\sigma_{\text{Mott}}} \cdot \overline{\rho_{LT}} \cdot f_{LT}. \tag{8}$$

Here $\overline{\cos(\phi_0)}$ and $\overline{\cos(\phi_1)}$ are averages for the settings centered around $\phi = 0^\circ$ and $\phi = 180^\circ$ respectively, C_{tot} contains all normalization factors, and $\overline{\sigma_{\text{Mott}}}$ is the averaged Mott cross section for the bin considered. This separation required that all kinematic variables except ϕ are identical. This is in general

not the case as can be seen from Fig. 7. Only the central bin approximately satisfies this condition.

In addition to the small overlap between the two ϕ settings, the cross section determined for each missing momentum bin differs slightly from the cross section corresponding to the averaged kinematics associated with this bin. This difference will also introduce a systematic error in the extracted response function and needs to be corrected.

To correct for these effects we have calculated the averaged cross section for each missing momentum bin. For one set of calculations we used PWIA and the momentum distribution calculated with the Paris potential, for the other set of calculations we interpolated the theoretical response functions that include FSI, MEC, and IC. These two calculations allow one also to estimate the model dependence for correction factors derived for the effects above.

The ratio between the cross section calculated for the averaged kinematics ($\sigma^{\rm calc}_{\rm kin_{av}}$) and the averaged cross section ($\overline{\sigma^{\rm calc}}$) for each bin can be used to correct the experimental cross section for bin centering ($\sigma^{\rm exp}_{bc}$)

$$\sigma^{\rm exp}_{\rm bc} = f_{\rm bc}\cdot\sigma^{\rm exp}, \quad f_{\rm bc} = \frac{\sigma^{\rm calc}_{\rm kin_{av}}}{\overline{\sigma^{\rm calc}}}. \tag{9}$$

Bin centering corrections (9) are typically of the order of a few percent and are larger at the edge of the acceptance compared to its center (Fig. 8). The largest shifts occur for the $\theta^{\rm c.m.}_{np} = 0^\circ$ data set. The ratios calculated using PWIA are considerably smaller and are also shown in Fig. 8.

The bin-centered, 'experimental' cross sections $\sigma^{\rm exp}_{\rm bc}$ (9) together with the corresponding averaged kinematics can be used for comparison with theory without the need to perform a Monte Carlo averaging of the theoretical cross sections over the full spectrometer acceptance. The drawback of bin center corrections is that one introduces a certain amount of model

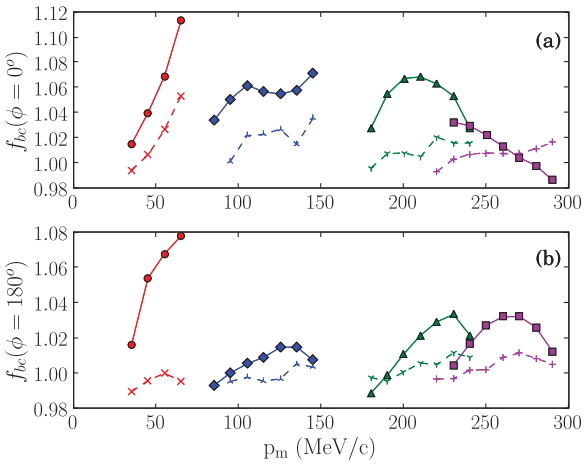

FIG. 8. (Color online) Ratio between the averaged ^{2}H$(e, e'p)n$ cross section for each missing momentum bin and the cross section calculated using the corresponding averaged kinematics. (a) Ratios for $\phi = 0^\circ$. (b) Ratios for $\phi = 180^\circ$. The full lines joining the solid symbols are calculated using the full theory while the dashed lines are calculated using PWIA. The ratios $f_{\rm bc}$ calculated with the full calculation are used to correct the experimental cross sections as described in the text.

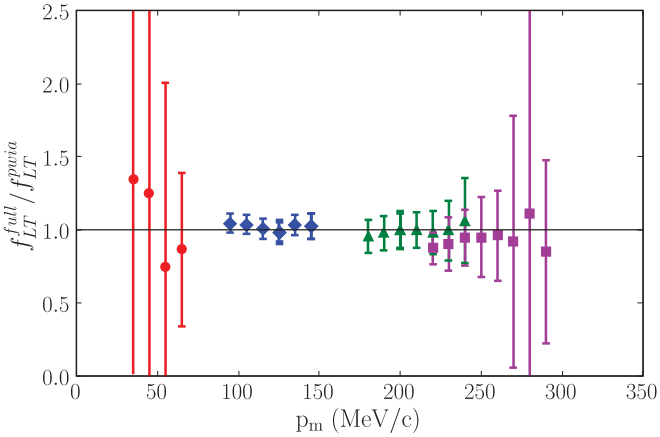

FIG. 9. (Color online) Ratio between the experimental values of the response function f_{LT} determined using the full calculation for all corrections and using PWIA for the corrections. For comparison the error bars indicate the relative error in f_{LT}.

dependence. Comparing the bin-centering corrections between the full calculation and PWIA gives an estimate of the model dependence of this approach (Figs. 8 and 9).

When we used the theoretical cross sections for the extraction of f_{LT} to test the extraction method we found deviations of up to 15% between the obtained value for f_{LT} and the theoretical one. This was due to the mismatch in the kinematic variables between the $\phi = 0^\circ$ and the $\phi = 180^\circ$ kinematic settings for each corresponding missing momentum bin. These differences affect especially the photon density matrix ρ_{ij} and the Mott cross section which should be independent of ϕ.

The same model used to determine the bin centering correction has therefore been applied in a second step to correct for these kinematic differences for each p_m bin as follows: we calculated the cross sections for exactly the same kinematics as the $\phi = 0^\circ$ data with ϕ changed to the appropriate values of the $\phi = 180^\circ$ data leading to $\sigma^{\rm calc}_m$. The experimental cross sections for the $\phi = 180^\circ$ data sets have then been corrected for the kinematic mismatch by multiplying them bin-wise by $\sigma^{\rm calc}_m/\sigma^{\rm calc}_{\rm kin_{av}}$:

$$\sigma^{\rm exp}_{{\rm bc},m,\phi=180} = \sigma^{\rm exp}_{{\rm bc},\phi=180}\cdot\frac{\sigma^{\rm calc}_m}{\sigma^{\rm calc}_{\rm kin_{av}}}. \tag{10}$$

The matched cross sections have then been used to determine f_{LT} and the asymmetry A_{LT} defined as

$$A_{LT} = \frac{(\sigma_{\phi=0^\circ} - \sigma_{\phi=180^\circ})}{(\sigma_{\phi=0^\circ} + \sigma_{\phi=180^\circ})}. \tag{11}$$

The experimental results for f_{LT} using the procedure described above are shown in Fig. 11 and the one for A_{LT} are shown in Fig. 12.

To estimate the effect of the model dependence of the entire procedure on the extraction of f_{LT} we have performed the same analysis using PWIA in order to calculate the theoretical cross sections. The ratio between f_{LT} obtained using the full calculation which includes FSI, MEC, IC, and R and f_{LT} obtained using PWIA is shown in Fig. 9. In general the observed deviations are considerably smaller than the error

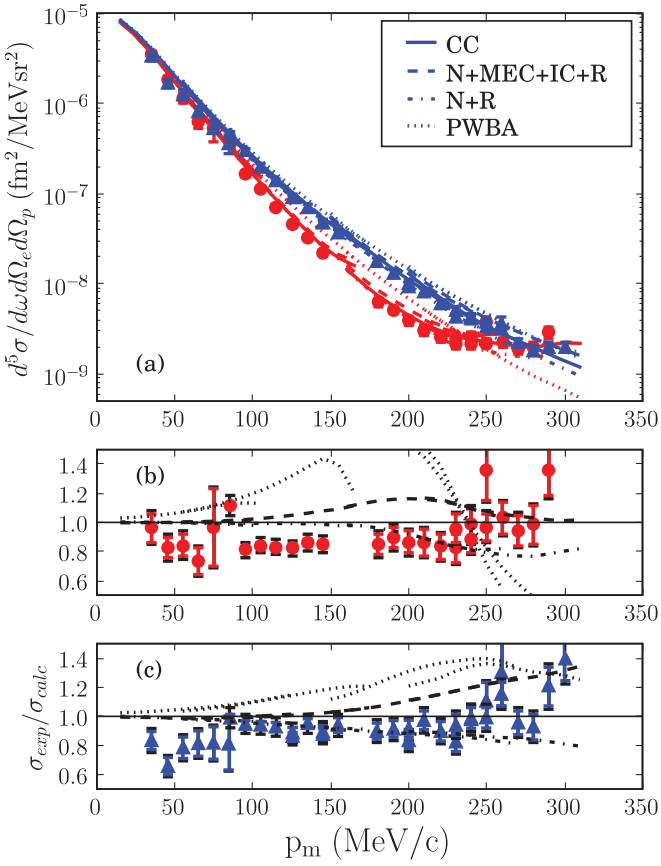

FIG. 10. (Color online) (a) Experimental cross sections as a function of missing momentum; red circles correspond to the $\phi = 0^\circ$ settings and blue triangles correspond to the $\phi = 180^\circ$ kinematics. The lines represent theoretical calculations [7]; coupled channel calculation (CC, solid), PWBA (dotted), FSI and relativistic corrections (N+R, dash-dot) and FSI, MEC, IC and relativistic corrections (N+MEC+IC+R, dashed). (b) Ratio between experimental cross sections and calculation for $\phi = 0^\circ$. (c) Ratio between experimental cross sections and calculation for $\phi = 180^\circ$. The labeling of the calculations is the same as for the top panel.

of f_{LT} and except for the edges of the acceptance smaller than 10%. For the comparisons with the calculations we always used those experimental values that have been extracted using the full calculation for the correction factors.

IV. RESULTS AND DISCUSSION

A comparison of the calculated cross sections to the experimental ones as a function of missing momentum is presented in Fig. 10. The red circles correspond to kinematic settings centered around $\phi = 0^\circ$ and the blue triangles correspond to kinematic settings centered around $\phi = 180^\circ$. In order to better compare the experimental cross sections to the calculated ones the ratio between experiment and calculation is shown in the lower two graphs in Fig. 10. While the general behavior of the cross sections as a function of missing momentum is well reproduced by the calculation, one finds that the experimental cross sections are generally of the order of 10 to 20% below the calculation especially for the $\phi = 0^\circ$ kinematics. This behavior

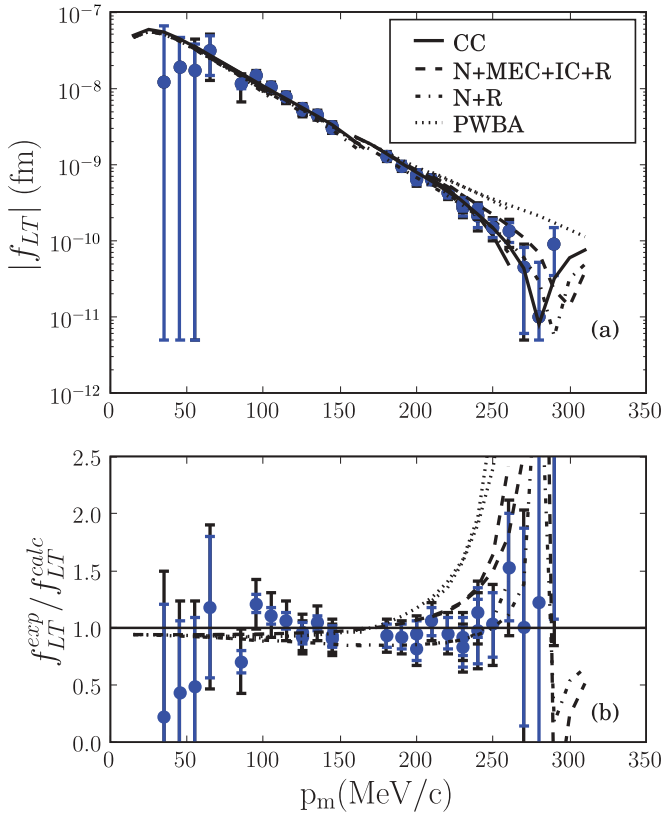

FIG. 11. (Color online) (a) Extracted interference response function f_{LT} as a function of missing momentum. The smaller error bar represents the statistical error and the larger one includes the systematic uncertainty. As in Fig. 10 the lines represent the theoretical calculations. (b) Ratio between experimental values of f_{LT} and calculations. The labeling of the calculations is the same as for (a).

is similar to what has been observed in other experiments as well and needs further study [2,4,5].

The coupled channel calculation [7], including explicit pionic degrees of freedom and using the Bonn-OBEPR potential seems to agree best with the experimental data (solid lines). This is the same calculation that was compared to experimental results in a determination of the interference response function

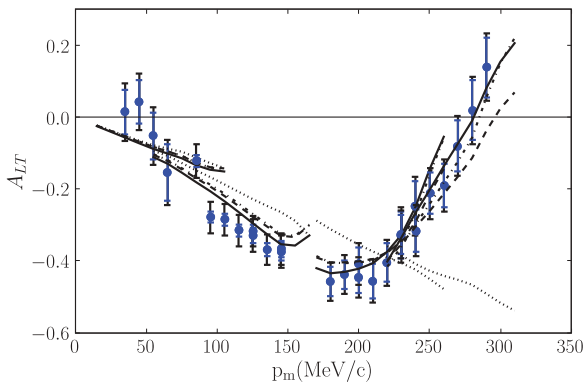

FIG. 12. (Color online) The asymmetry A_{LT} compared to the calculation. The labeling of the curves is the same as in Figs. 10 and 11. Both the statistical and the total errors are indicated.

f_{TT} in the delta region by Pellegrino *et al.* [12]. Among the impulse approximation based calculations the best agreement is obtained by the calculation including FSI and R (N+R), while the one including all contributions (N+MEC+IC+R), systematically over-predicts the cross sections for $\phi = 0^\circ$ as well as for $\phi = 180^\circ$. In Fig. 12 the extracted asymmetry A_{LT} (11) is compared to the one determined from the coupled channel model (CC, solid curve). The calculation systematically deviates from the experiment in the same region where the cross sections deviate. This indicates that this discrepancy is not due to an overall normalization factor in the cross sections since an overall factor would cancel in A_{LT}. The observed deviation could be due to a discrepancy in the interference response function or the longitudinal (f_L) and/or the transverse (f_T) responses. We compared the extracted response function f_{LT} to the one calculated from the coupled channel calculation (Fig. 11) and found that the calculation agrees well with the experiment within the experimental error bars. This suggests that the observed differences in the cross section is not due to a difference in f_{LT} but due to a discrepancy in the longitudinal/transverse responses.

This is in agreement with the experiments mentioned in the introduction that extracted f_L and f_T and found that the experimental value of f_L is systematically smaller than the calculated f_L [16,18].

V. SUMMARY AND CONCLUSION

In summary, we have measured the ^{2}H$(e, e'p)n$ cross section for missing momenta up to 290 MeV/c at $\phi = 0^\circ$ and $\phi = 180^\circ$ and extracted the interference response function f_{LT}. This response is well reproduced by the coupled channel calculation using the Bonn potential. The measured cross sections are systematically below the calculations by 10–20% for missing momenta between 100 MeV/c and 200 MeV/c. This same behavior can also be observed in other experiments [2,4,5]. The fact that the extracted experimental values for f_{LT} agree well with the calculation leads to the conclusion that the cross section deviations at lower missing momenta are due to differences in the longitudinal and/or the transverse responses. To further investigate this issue would require an L/T separation which has not been carried out for this kinematics to date.

ACKNOWLEDGMENTS

Numerical results in electronic form are available from the first author. This work was supported in part by the Department of Energy, DOE grant DE-FG02-99ER41065 and by the Deutsche Forschungsgemeinschaft (SFB 201).

APPENDIX: KINEMATICS TABLES AND NUMERICAL RESULTS

Tables III–X contain the average kinematic setting for each bin in missing momentum together with the experimental cross section, the bin corrected cross section and the statistical and systematic errors. Tables XI–XIV contain the extracted response function f_{LT} including statistical and systematic errors, the asymmetry A_{LT} including all its errors and the corrected experimental cross section for the $\phi = 180^\circ$ setting matched to the kinematics at $\phi = 0^\circ$ as described in the text above.

TABLE III. Averaged kinematics and cross sections for setting: I.

p_m (MeV/c)	θ_e (°)	ω (MeV)	q_{lab} (MeV/c)	θ_{pq}^{lab} (°)	ϕ_{pq} (°)	p_f (MeV/c)	σ_{exp} ($\frac{\text{fm}^2}{\text{MeV·Sr}^2}$)	$\sigma_{\text{exp}}^{\text{bincorr.}}$ ($\frac{\text{fm}^2}{\text{MeV·Sr}^2}$)	$\pm\Delta\sigma_{\text{stat}}$ ($\frac{\text{fm}^2}{\text{MeV·Sr}^2}$)	$\pm\Delta\sigma_{\text{sys}}$ ($\frac{\text{fm}^2}{\text{MeV·Sr}^2}$)
35.0	45.17	190.0	609.5	3.07	32.91	621.3	3.49×10^{-6}	3.44×10^{-6}	3.5×10^{-7}	2.4×10^{-7}
45.0	45.15	193.3	609.0	3.85	32.46	626.4	1.90×10^{-6}	1.83×10^{-6}	1.6×10^{-7}	1.3×10^{-7}
55.0	45.07	196.3	607.9	4.62	33.55	630.9	1.22×10^{-6}	1.15×10^{-6}	1.2×10^{-7}	7.9×10^{-8}
65.0	44.99	200.0	606.7	5.34	38.75	636.3	6.89×10^{-7}	6.19×10^{-7}	8.4×10^{-8}	4.4×10^{-8}
75.0	44.88	201.7	605.3	6.23	45.38	637.9	5.88×10^{-7}	5.18×10^{-7}	1.6×10^{-7}	3.7×10^{-8}

TABLE IV. Averaged kinematics and cross sections for setting: II.

p_m (MeV/c)	θ_e (°)	ω (MeV)	q_{lab} (MeV/c)	θ_{pq}^{lab} (°)	ϕ_{pq} (°)	p_f (MeV/c)	σ_{exp} ($\frac{\text{fm}^2}{\text{MeV·Sr}^2}$)	$\sigma_{\text{exp}}^{\text{bincorr.}}$ ($\frac{\text{fm}^2}{\text{MeV·Sr}^2}$)	$\pm\Delta\sigma_{\text{stat}}$ ($\frac{\text{fm}^2}{\text{MeV·Sr}^2}$)	$\pm\Delta\sigma_{\text{sys}}$ ($\frac{\text{fm}^2}{\text{MeV·Sr}^2}$)
85.0	44.92	199.4	605.8	7.48	8.35	632.3	3.67×10^{-7}	3.55×10^{-7}	4.6×10^{-9}	2.3×10^{-8}
95.0	44.91	202.6	605.5	8.30	8.39	636.3	1.73×10^{-7}	1.65×10^{-7}	3.3×10^{-9}	1.1×10^{-8}
105.0	44.90	204.8	605.3	9.20	8.27	638.3	1.17×10^{-7}	1.11×10^{-7}	2.7×10^{-9}	7.3×10^{-9}
115.0	44.89	204.7	605.2	10.25	8.27	636.0	7.51×10^{-8}	7.11×10^{-8}	1.4×10^{-9}	4.7×10^{-9}
125.0	44.89	204.5	605.2	11.29	8.19	633.4	4.91×10^{-8}	4.66×10^{-8}	1.1×10^{-9}	3.1×10^{-9}
135.0	44.89	204.2	605.3	12.33	8.15	630.3	3.46×10^{-8}	3.27×10^{-8}	8.9×10^{-10}	2.2×10^{-9}
145.0	44.86	200.4	605.2	13.50	8.27	621.1	2.36×10^{-8}	2.21×10^{-8}	6.6×10^{-10}	1.5×10^{-9}

TABLE V. Averaged kinematics and cross sections for setting: III.

p_m (MeV/c)	θ_e (°)	ω (MeV)	$q_{\rm lab}$ (MeV/c)	$\theta_{pq}^{\rm lab}$ (°)	ϕ_{pq} (°)	p_f (MeV/c)	$\sigma_{\rm exp}$ ($\frac{\rm fm^2}{\rm MeV\cdot Sr^2}$)	$\sigma_{\rm exp}^{\rm bincorr.}$ ($\frac{\rm fm^2}{\rm MeV\cdot Sr^2}$)	$\pm\Delta\sigma_{\rm stat}$ ($\frac{\rm fm^2}{\rm MeV\cdot Sr^2}$)	$\pm\Delta\sigma_{\rm sys}$ ($\frac{\rm fm^2}{\rm MeV\cdot Sr^2}$)
180.0	44.89	204.9	605.1	16.88	7.52	618.2	6.48×10^{-9}	6.30×10^{-9}	5.4×10^{-10}	4.0×10^{-10}
190.0	44.89	201.1	605.5	18.02	7.52	607.7	5.40×10^{-9}	5.12×10^{-9}	4.2×10^{-10}	3.4×10^{-10}
200.0	44.90	200.4	605.6	19.05	7.52	602.6	4.11×10^{-9}	3.85×10^{-9}	3.6×10^{-10}	2.6×10^{-10}
210.0	44.90	201.2	605.6	20.05	7.39	600.1	3.29×10^{-9}	3.08×10^{-9}	3.3×10^{-10}	2.0×10^{-10}
220.0	44.90	201.1	605.6	21.08	7.25	595.9	2.68×10^{-9}	2.52×10^{-9}	2.8×10^{-10}	1.7×10^{-10}
230.0	44.90	200.8	605.6	22.12	7.11	590.8	2.31×10^{-9}	2.19×10^{-9}	2.8×10^{-10}	1.4×10^{-10}
240.0	44.90	197.9	605.8	23.21	7.16	581.1	2.60×10^{-9}	2.52×10^{-9}	3.0×10^{-10}	1.6×10^{-10}
250.0	44.92	192.5	606.4	24.31	7.16	566.3	3.69×10^{-9}	3.69×10^{-9}	5.4×10^{-10}	2.3×10^{-10}

TABLE VI. Averaged kinematics and cross sections for setting: IV.

p_m (MeV/c)	θ_e (°)	ω (MeV)	$q_{\rm lab}$ (MeV/c)	$\theta_{pq}^{\rm lab}$ (°)	ϕ_{pq} (°)	p_f (MeV/c)	$\sigma_{\rm exp}$ ($\frac{\rm fm^2}{\rm MeV\cdot Sr^2}$)	$\sigma_{\rm exp}^{\rm bincorr.}$ ($\frac{\rm fm^2}{\rm MeV\cdot Sr^2}$)	$\pm\Delta\sigma_{\rm stat}$ ($\frac{\rm fm^2}{\rm MeV\cdot Sr^2}$)	$\pm\Delta\sigma_{\rm sys}$ ($\frac{\rm fm^2}{\rm MeV\cdot Sr^2}$)
230.0	45.00	202.3	606.5	22.06	6.83	593.8	2.56×10^{-9}	2.48×10^{-9}	2.5×10^{-10}	1.6×10^{-10}
240.0	45.02	200.5	607.0	23.13	6.88	585.8	2.22×10^{-9}	2.16×10^{-9}	2.4×10^{-10}	1.4×10^{-10}
250.0	45.03	200.4	607.1	24.17	6.69	580.8	2.25×10^{-9}	2.20×10^{-9}	2.1×10^{-10}	1.4×10^{-10}
260.0	45.03	200.3	607.1	25.22	6.43	575.6	2.24×10^{-9}	2.21×10^{-9}	2.3×10^{-10}	1.4×10^{-10}
270.0	45.03	200.6	607.1	26.27	6.17	571.1	1.93×10^{-9}	1.92×10^{-9}	2.2×10^{-10}	1.2×10^{-10}
280.0	45.05	200.5	607.2	27.33	5.96	565.7	1.94×10^{-9}	1.94×10^{-9}	2.6×10^{-10}	1.2×10^{-10}
290.0	45.10	196.1	608.1	28.43	5.96	551.8	2.82×10^{-9}	2.86×10^{-9}	3.6×10^{-10}	1.8×10^{-10}

TABLE VII. Averaged kinematics and cross sections for setting: V.

p_m (MeV/c)	θ_e (°)	ω (MeV)	$q_{\rm lab}$ (MeV/c)	$\theta_{pq}^{\rm lab}$ (°)	ϕ_{pq} (°)	p_f (MeV/c)	$\sigma_{\rm exp}$ ($\frac{\rm fm^2}{\rm MeV\cdot Sr^2}$)	$\sigma_{\rm exp}^{\rm bincorr.}$ ($\frac{\rm fm^2}{\rm MeV\cdot Sr^2}$)	$\pm\Delta\sigma_{\rm stat}$ ($\frac{\rm fm^2}{\rm MeV\cdot Sr^2}$)	$\pm\Delta\sigma_{\rm sys}$ ($\frac{\rm fm^2}{\rm MeV\cdot Sr^2}$)
35.0	45.20	191.7	609.7	2.95	145.04	624.5	3.38×10^{-6}	3.33×10^{-6}	2.5×10^{-7}	2.2×10^{-7}
45.0	45.15	197.7	608.5	3.39	144.54	634.4	1.75×10^{-6}	1.66×10^{-6}	1.6×10^{-7}	1.1×10^{-7}
55.0	45.13	203.7	607.7	3.77	144.67	644.2	1.34×10^{-6}	1.25×10^{-6}	1.3×10^{-7}	8.7×10^{-8}
65.0	45.09	209.6	606.9	4.12	145.17	653.5	8.89×10^{-7}	8.25×10^{-7}	9.5×10^{-8}	5.8×10^{-8}
75.0	44.99	214.0	605.5	4.69	145.29	659.8	5.88×10^{-7}	5.38×10^{-7}	8.0×10^{-8}	3.8×10^{-8}
85.0	44.94	216.4	604.8	5.64	144.87	662.6	3.86×10^{-7}	3.55×10^{-7}	8.5×10^{-8}	2.5×10^{-8}

TABLE VIII. Averaged kinematics and cross sections for setting: VI.

p_m (MeV/c)	θ_e (°)	ω (MeV)	$q_{\rm lab}$ (MeV/c)	$\theta_{pq}^{\rm lab}$ (°)	ϕ_{pq} (°)	p_f (MeV/c)	$\sigma_{\rm exp}$ ($\frac{\rm fm^2}{\rm MeV\cdot Sr^2}$)	$\sigma_{\rm exp}^{\rm bincorr.}$ ($\frac{\rm fm^2}{\rm MeV\cdot Sr^2}$)	$\pm\Delta\sigma_{\rm stat}$ ($\frac{\rm fm^2}{\rm MeV\cdot Sr^2}$)	$\pm\Delta\sigma_{\rm sys}$ ($\frac{\rm fm^2}{\rm MeV\cdot Sr^2}$)
85.0	44.88	191.9	606.0	7.86	171.53	619.0	4.60×10^{-7}	4.63×10^{-7}	1.3×10^{-8}	2.9×10^{-8}
95.0	44.89	194.9	605.8	8.73	171.61	622.5	2.96×10^{-7}	2.96×10^{-7}	7.7×10^{-9}	1.9×10^{-8}
105.0	44.90	197.9	605.7	9.60	171.65	626.0	2.02×10^{-7}	2.00×10^{-7}	5.3×10^{-9}	1.3×10^{-8}
115.0	44.90	200.5	605.6	10.48	171.69	628.6	1.38×10^{-7}	1.37×10^{-7}	4.5×10^{-9}	8.7×10^{-9}
125.0	44.90	203.2	605.4	11.36	171.69	631.0	9.09×10^{-8}	8.96×10^{-8}	2.7×10^{-9}	5.7×10^{-9}
125.0	44.90	203.2	605.4	11.36	171.69	631.0	9.09×10^{-8}	9.22×10^{-8}	2.7×10^{-9}	5.7×10^{-9}
125.0	44.90	203.2	605.4	11.36	171.69	631.0	9.35×10^{-8}	8.96×10^{-8}	3.7×10^{-9}	5.9×10^{-9}
125.0	44.90	203.2	605.4	11.36	171.69	631.0	9.35×10^{-8}	9.22×10^{-8}	3.7×10^{-9}	5.9×10^{-9}
135.0	44.91	206.4	605.3	12.21	171.65	634.4	7.16×10^{-8}	7.05×10^{-8}	2.4×10^{-9}	4.5×10^{-9}
145.0	44.92	211.1	605.0	12.97	171.65	640.3	4.75×10^{-8}	4.72×10^{-8}	2.0×10^{-9}	3.0×10^{-9}
145.0	44.92	211.1	605.0	12.97	171.65	640.3	4.75×10^{-8}	4.81×10^{-8}	2.0×10^{-9}	3.0×10^{-9}
145.0	44.92	211.1	605.0	12.97	171.65	640.3	4.84×10^{-8}	4.72×10^{-8}	2.3×10^{-9}	3.0×10^{-9}
145.0	44.92	211.1	605.0	12.97	171.65	640.3	4.84×10^{-8}	4.81×10^{-8}	2.3×10^{-9}	3.0×10^{-9}
155.0	44.92	215.2	604.7	13.77	171.69	644.9	3.71×10^{-8}	3.72×10^{-8}	2.0×10^{-9}	2.3×10^{-9}

TABLE IX. Averaged kinematics and cross sections for setting: VIII.

p_m (MeV/c)	θ_e (°)	ω (MeV)	$q_{\rm lab}$ (MeV/c)	$\theta_{pq}^{\rm lab}$ (°)	ϕ_{pq} (°)	p_f (MeV/c)	$\sigma_{\rm exp}$ ($\frac{\rm fm^2}{\rm MeV\cdot Sr^2}$)	$\sigma_{\rm exp}^{\rm bincorr.}$ ($\frac{\rm fm^2}{\rm MeV\cdot Sr^2}$)	$\pm\Delta\sigma_{\rm stat}$ ($\frac{\rm fm^2}{\rm MeV\cdot Sr^2}$)	$\pm\Delta\sigma_{\rm sys}$ ($\frac{\rm fm^2}{\rm MeV\cdot Sr^2}$)
180.0	44.87	191.0	606.0	17.22	172.10	592.9	1.75×10^{-8}	1.77×10^{-8}	1.1×10^{-9}	1.1×10^{-9}
190.0	44.89	194.5	605.9	18.17	172.14	595.6	1.34×10^{-8}	1.34×10^{-8}	8.4×10^{-10}	8.3×10^{-10}
200.0	44.89	197.7	605.7	19.12	172.10	597.8	1.02×10^{-8}	1.01×10^{-8}	6.4×10^{-10}	6.4×10^{-10}
200.0	44.89	197.7	605.7	19.12	172.10	597.8	1.02×10^{-8}	9.23×10^{-9}	6.4×10^{-10}	6.4×10^{-10}
200.0	44.89	197.7	605.7	19.12	172.10	597.8	9.33×10^{-9}	1.01×10^{-8}	6.1×10^{-10}	5.8×10^{-10}
200.0	44.89	197.7	605.7	19.12	172.10	597.8	9.33×10^{-9}	9.23×10^{-9}	6.1×10^{-10}	5.8×10^{-10}
210.0	44.90	200.9	605.5	20.06	172.14	599.6	8.43×10^{-9}	8.25×10^{-9}	5.6×10^{-10}	5.2×10^{-10}
220.0	44.90	202.8	605.4	21.04	172.14	599.1	6.10×10^{-9}	5.93×10^{-9}	4.5×10^{-10}	3.8×10^{-10}
230.0	44.91	203.6	605.5	22.05	172.14	596.2	4.44×10^{-9}	4.29×10^{-9}	3.6×10^{-10}	2.8×10^{-10}
240.0	44.93	206.8	605.5	23.00	172.14	597.7	4.15×10^{-9}	4.06×10^{-9}	3.7×10^{-10}	2.6×10^{-10}
250.0	44.94	212.1	605.2	23.88	172.14	603.2	3.70×10^{-9}	3.71×10^{-9}	4.2×10^{-10}	2.3×10^{-10}
260.0	44.97	219.4	605.1	24.65	172.31	612.3	3.59×10^{-9}	3.63×10^{-9}	6.3×10^{-10}	2.2×10^{-10}

TABLE X. Averaged kinematics and cross sections for setting: VIII.

p_m (MeV/c)	θ_e (°)	ω (MeV)	$q_{\rm lab}$ (MeV/c)	$\theta_{pq}^{\rm lab}$ (°)	ϕ_{pq} (°)	p_f (MeV/c)	$\sigma_{\rm exp}$ ($\frac{\rm fm^2}{\rm MeV\cdot Sr^2}$)	$\sigma_{\rm exp}^{\rm bincorr.}$ ($\frac{\rm fm^2}{\rm MeV\cdot Sr^2}$)	$\pm\Delta\sigma_{\rm stat}$ ($\frac{\rm fm^2}{\rm MeV\cdot Sr^2}$)	$\pm\Delta\sigma_{\rm sys}$ ($\frac{\rm fm^2}{\rm MeV\cdot Sr^2}$)
230.0	45.00	194.3	607.2	22.20	172.39	578.8	5.13×10^{-9}	5.10×10^{-9}	3.8×10^{-10}	3.2×10^{-10}
240.0	45.00	198.1	606.9	23.18	172.39	581.4	4.28×10^{-9}	4.21×10^{-9}	3.1×10^{-10}	2.7×10^{-10}
250.0	45.01	201.1	606.7	24.16	172.39	582.2	3.46×10^{-9}	3.37×10^{-9}	2.5×10^{-10}	2.2×10^{-10}
260.0	45.02	202.1	606.8	25.19	172.39	579.2	3.33×10^{-9}	3.23×10^{-9}	2.3×10^{-10}	2.1×10^{-10}
270.0	45.03	202.5	606.9	26.24	172.44	574.6	2.31×10^{-9}	2.23×10^{-9}	2.0×10^{-10}	1.4×10^{-10}
280.0	45.06	204.5	607.0	27.25	172.48	573.3	1.87×10^{-9}	1.82×10^{-9}	1.8×10^{-10}	1.2×10^{-10}
290.0	45.09	208.8	607.0	28.22	172.48	576.2	2.01×10^{-9}	1.99×10^{-9}	2.3×10^{-10}	1.3×10^{-10}
300.0	45.10	214.1	606.8	29.16	172.44	580.8	1.95×10^{-9}	1.96×10^{-9}	2.1×10^{-10}	1.2×10^{-10}

TABLE XI. f_{LT} and A_{LT} from settings: I and V.

p_m (MeV/c)	f_{LT} (fm)	$\Delta f_{LT_{\rm stat}}$ (fm)	$\Delta f_{LT_{\rm sys}}$ (fm)	A_{LT}	$\Delta A_{LT,\rm stat}$	$\Delta A_{LT,\rm sys}$	$\sigma_{{\rm exp},m}$ ($\frac{\rm fm^2}{\rm MeV\cdot Sr^2}$)
35.0	1.20×10^{-8}	5.4×10^{-8}	4.4×10^{-8}	1.40×10^{-2}	6.2×10^{-2}	5.1×10^{-2}	3.34×10^{-6}
45.1	1.92×10^{-8}	2.8×10^{-8}	2.2×10^{-8}	4.23×10^{-2}	6.2×10^{-2}	4.8×10^{-2}	1.68×10^{-6}
55.0	-1.69×10^{-8}	2.1×10^{-8}	1.5×10^{-8}	-5.27×10^{-2}	6.6×10^{-2}	4.7×10^{-2}	1.27×10^{-6}
65.0	-3.14×10^{-8}	1.6×10^{-8}	9.6×10^{-9}	-1.54×10^{-1}	7.9×10^{-2}	4.5×10^{-2}	8.43×10^{-7}

TABLE XII. f_{LT} and A_{LT} from settings: II and VI.

p_m (MeV/c)	f_{LT} (fm)	$\Delta f_{LT_{\rm stat}}$ (fm)	$\Delta f_{LT_{\rm sys}}$ (fm)	A_{LT}	$\Delta A_{LT,\rm stat}$	$\Delta A_{LT,\rm sys}$	$\sigma_{{\rm exp},m}$ ($\frac{\rm fm^2}{\rm MeV\cdot Sr^2}$)
85.0	-1.12×10^{-8}	1.6×10^{-9}	4.1×10^{-9}	-1.22×10^{-1}	1.5×10^{-2}	4.4×10^{-2}	4.54×10^{-7}
95.1	-1.47×10^{-8}	9.5×10^{-10}	2.4×10^{-9}	-2.79×10^{-1}	1.5×10^{-2}	4.1×10^{-2}	2.92×10^{-7}
105.1	-1.03×10^{-8}	6.8×10^{-10}	1.7×10^{-9}	-2.85×10^{-1}	1.6×10^{-2}	4.1×10^{-2}	1.99×10^{-7}
115.1	-7.68×10^{-9}	5.4×10^{-10}	1.1×10^{-9}	-3.15×10^{-1}	1.7×10^{-2}	4.0×10^{-2}	1.36×10^{-7}
125.1	-5.09×10^{-9}	3.3×10^{-10}	7.5×10^{-10}	-3.16×10^{-1}	1.6×10^{-2}	4.0×10^{-2}	8.97×10^{-8}
125.1	-5.09×10^{-9}	3.3×10^{-10}	7.5×10^{-10}	-3.16×10^{-1}	1.6×10^{-2}	4.0×10^{-2}	9.22×10^{-8}
125.1	-5.39×10^{-9}	4.5×10^{-10}	7.7×10^{-10}	-3.29×10^{-1}	2.0×10^{-2}	4.0×10^{-2}	8.97×10^{-8}
125.1	-5.39×10^{-9}	4.5×10^{-10}	7.7×10^{-10}	-3.29×10^{-1}	2.0×10^{-2}	4.0×10^{-2}	9.22×10^{-8}
135.1	-4.49×10^{-9}	3.0×10^{-10}	5.8×10^{-10}	-3.67×10^{-1}	1.8×10^{-2}	3.8×10^{-2}	7.06×10^{-8}
145.1	-2.96×10^{-9}	2.5×10^{-10}	3.8×10^{-10}	-3.66×10^{-1}	2.2×10^{-2}	3.8×10^{-2}	4.76×10^{-8}
145.1	-2.96×10^{-9}	2.5×10^{-10}	3.8×10^{-10}	-3.66×10^{-1}	2.2×10^{-2}	3.8×10^{-2}	4.85×10^{-8}
145.1	-3.07×10^{-9}	2.7×10^{-10}	3.9×10^{-10}	-3.74×10^{-1}	2.4×10^{-2}	3.8×10^{-2}	4.76×10^{-8}
145.1	-3.07×10^{-9}	2.7×10^{-10}	3.9×10^{-10}	-3.74×10^{-1}	2.4×10^{-2}	3.8×10^{-2}	4.85×10^{-8}

TABLE XIII. f_{LT} and A_{LT} from settings: III and VII.

p_m (MeV/c)	f_{LT} (fm)	$\Delta f_{LT_{\text{stat}}}$ (fm)	$\Delta f_{LT_{\text{sys}}}$ (fm)	A_{LT}	$\Delta A_{LT,\text{stat}}$	$\Delta A_{LT,\text{sys}}$	$\sigma_{\text{exp},m}$ ($\frac{\text{fm}^2}{\text{MeV}\cdot\text{Sr}^2}$)
180.0	-1.29×10^{-9}	1.4×10^{-10}	1.4×10^{-10}	-4.57×10^{-1}	4.1×10^{-2}	3.5×10^{-2}	1.69×10^{-8}
190.0	-9.57×10^{-10}	1.1×10^{-10}	1.1×10^{-10}	-4.37×10^{-1}	4.0×10^{-2}	3.6×10^{-2}	1.31×10^{-8}
200.0	-7.47×10^{-10}	8.7×10^{-11}	8.1×10^{-11}	-4.45×10^{-1}	4.3×10^{-2}	3.5×10^{-2}	1.00×10^{-8}
200.0	-7.47×10^{-10}	8.7×10^{-11}	8.1×10^{-11}	-4.45×10^{-1}	4.3×10^{-2}	3.5×10^{-2}	9.15×10^{-9}
200.0	-6.39×10^{-10}	8.3×10^{-11}	7.5×10^{-11}	-4.07×10^{-1}	4.6×10^{-2}	3.7×10^{-2}	1.00×10^{-8}
200.0	-6.39×10^{-10}	8.3×10^{-11}	7.5×10^{-11}	-4.07×10^{-1}	4.6×10^{-2}	3.7×10^{-2}	9.15×10^{-9}
210.1	-6.31×10^{-10}	7.7×10^{-11}	6.7×10^{-11}	-4.56×10^{-1}	4.8×10^{-2}	3.5×10^{-2}	8.25×10^{-9}
220.1	-4.22×10^{-10}	6.3×10^{-11}	5.0×10^{-11}	-4.04×10^{-1}	5.3×10^{-2}	3.7×10^{-2}	5.95×10^{-9}
230.1	-2.65×10^{-10}	5.5×10^{-11}	3.7×10^{-11}	-3.28×10^{-1}	6.5×10^{-2}	3.9×10^{-2}	4.33×10^{-9}
240.1	-2.05×10^{-10}	5.9×10^{-11}	3.7×10^{-11}	-2.48×10^{-1}	6.9×10^{-2}	4.1×10^{-2}	4.19×10^{-9}

TABLE XIV. f_{LT} and A_{LT} from settings: IV and VIII.

p_m (MeV/c)	f_{LT} (fm)	$\Delta f_{LT_{\text{stat}}}$ (fm)	$\Delta f_{LT_{\text{sys}}}$ (fm)	A_{LT}	$\Delta A_{LT,\text{stat}}$	$\Delta A_{LT,\text{sys}}$	$\sigma_{\text{exp},m}$ ($\frac{\text{fm}^2}{\text{MeV}\cdot\text{Sr}^2}$)
230.0	-3.02×10^{-10}	5.5×10^{-11}	4.3×10^{-11}	-3.26×10^{-1}	5.5×10^{-2}	3.9×10^{-2}	4.88×10^{-9}
240.0	-2.51×10^{-10}	4.8×10^{-11}	3.7×10^{-11}	-3.16×10^{-1}	5.9×10^{-2}	4.0×10^{-2}	4.15×10^{-9}
250.0	-1.50×10^{-10}	4.1×10^{-11}	3.2×10^{-11}	-2.12×10^{-1}	5.7×10^{-2}	4.2×10^{-2}	3.38×10^{-9}
260.0	-1.34×10^{-10}	4.1×10^{-11}	3.1×10^{-11}	-1.91×10^{-1}	6.0×10^{-2}	4.2×10^{-2}	3.25×10^{-9}
270.1	-4.37×10^{-11}	3.8×10^{-11}	2.4×10^{-11}	-8.03×10^{-2}	7.0×10^{-2}	4.4×10^{-2}	2.26×10^{-9}
280.0	9.76×10^{-12}	4.2×10^{-11}	2.2×10^{-11}	1.95×10^{-2}	8.3×10^{-2}	4.4×10^{-2}	1.87×10^{-9}
290.0	9.07×10^{-11}	5.7×10^{-11}	2.9×10^{-11}	1.39×10^{-1}	8.3×10^{-2}	4.3×10^{-2}	2.17×10^{-9}

[1] T. de Forest, Nucl. Phys. **A392**, 232 (1983).
[2] M. Bernheim *et al*., Nucl. Phys. **A365**, 349 (1981).
[3] S. Turck-Chieze *et al*., Phys. Lett. **B142**, 145 (1984).
[4] K. I. Blomqvist *et al*., Phys. Lett. **B429**, 33 (1998).
[5] P. E Ulmer *et al*., Phys. Rev. Lett. **89**, 062301 (2002).
[6] H. Arenhövel, Nucl. Phys. **A384**, 287 (1982).
[7] H. Arenhövel, W. Leidemann, and L. Tomusiak, Eur. Phys. J. A **23**, 147 (2005).
[8] T. W. Donnelly and A. S. Raskin, Ann. Phys. (NY) **169**, 247 (1986).
[9] A. S. Raskin and T. W. Donnelly, Ann. Phys. (NY) **191**, 78 (1989).
[10] A. S. Raskin and T. W. Donnelly, Ann. Phys. (NY) **197**, 202 (1990).
[11] Z.-L. Zhou *et al*., Phys. Rev. Lett. **87**, 172301 (2001).
[12] A. Pellegrino *et al*., Phys. Rev. Lett. **78**, 4011 (1997).
[13] Z.-L. Zhou *et al*., Proccedings of the MIT-Bates Workshop (1998).
[14] M. van der Schaar *et al*., Phys. Rev. Lett. **66**, 2855 (1991).
[15] M. van der Schaar *et al*., Phys. Rev. Lett. **68**, 776 (1992).
[16] D. Jordan *et al*., Phys. Rev. Lett. **76**, 1579 (1996).
[17] W.-J. Kasdorp *et al*., Phys. Lett. **B393**, 42 (1997).
[18] J. E. Ducret *et al*., Phys. Rev. C **49**, 1783 (1994).
[19] H. J. Bulten *et al*., Phys. Rev. Lett. **74**, 4775 (1995).
[20] K. I. Blomqvist *et al*., Nucl. Instrum. Methods A **403**, 263 (1998).
[21] S. Platchkov *et al*., Nucl. Phys. **A510**, 740 (1990).
[22] S. Auffret *et al*., Phys. Rev. Lett. **54**, 649 (1985).